Chapter 6

Chemical Modification of Oligonucleotides: A Novel Approach Towards Gene Targeting

Hidetaka Torigoe and Takeshi Imanishi

Additional information is available at the end of the chapter

http://dx.doi.org/10.5772/50393

1. Introduction

Artificial regulation of gene expression is quite important for basic study to analyze unknown biological functions of target genes. Comparison of phenotypes with and without knockdown of expression level of the target genes may be helpful to reveal unknown biological functions of the target genes. Artificial regulation of gene expression is also important for therapeutic applications to reduce expression level of mutated target genes. Knockdown of expression level of the mutated target genes may be useful to avoid undesirable effects produced by the mutated target genes. Antisense and antigene technologies are powerful tools to artificially regulate target gene expression. In antisense technology, a single-stranded oligonucleotide added from outside may bind with target mRNA to form oligonucleotide-RNA duplex[1,2]. The formed duplex may inhibit ribosome-mediated translation of target mRNA due to its steric hindrance, or RNaseH may cleave target mRNA in the formed duplex, which may result in reduction of expression level of target mRNA in both cases[1,2]. In antigene technology, a single-stranded homopyrimidine triplex-forming oligonucleotide (TFO) added from outside may bind with homopurine-homopyrimidine stretch in target duplex DNA by Hoogsteen hydrogen bonding to form pyrimidine motif triplex, where T•A:T and C^+•G:C base triplets are formed[3,4]. The formed triplex inhibits RNA polymerase and transcription factors-mediated transcription of target gene due to its steric hindrance, which may result in downregulation of expression level of target gene[3,4].

Serious difficulties, such as poor binding ability of added oligonucleotides with target mRNA or target duplex DNA[5-7], and low stability of added oligonucleotides against nuclease degradation[8], may limit practical applications of the antisense and antigene technologies *in vivo*. Many kinds of chemically modified oligonucleotides have been developed to overcome these serious difficulties[9]. In this context, we have developed a

novel class of chemical modification of nucleic acids, 2′-*O*,4′-*C*-aminomethylene bridged nucleic acid (2′,4′-BNA^{NC}), in which 2′-O and 4′-C of the sugar moiety are bridged with the aminomethylene chain (Figure 1a)[10,11]. 2′,4′-BNA^{NC}-modified oligonucleotides showed higher binding affinity with target mRNA[11], stronger binding ability with target duplex DNA to form triplex[10-13], and higher stability against nuclease degradation than the corresponding unmodified oligonucleotides[11-13]. These excellent properties of 2′,4′-BNA^{NC}-modification of oligonucleotides may be favorable for their practical applications to the antisense and antigene technologies.

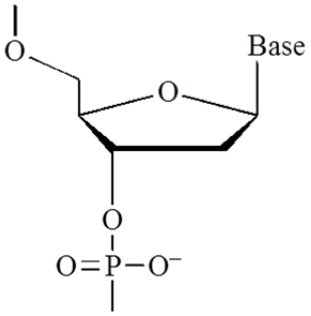

Phosphodiester (PO)

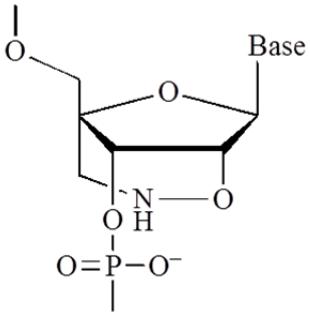

2′-*O*,4′-*C*-aminomethylene bridged nucleic acid (2′,4′-BNA^{NC})

(a)

```
Forward strand
F12         5′-d(GCGTTTTTTGCT)-3′
F12-1       5′-d(GCGTTTTTTGCT)-3′
F12-31      5′-d(GCGTTTTTTGCT)-3′
F12-32      5′-d(GCGTTTTTTGCT)-3′
F12-6       5′-d(GCGTTTTTTGCT)-3′
Complementary strand
R12R        3′-r(CGCAAAAAACGA)-5′
R12X        3′-r(CGCAAXAAACGA)-5′(X=A, U, G, C)
R12D        3′-d(CGCAAAAAACGA)-3′
T: T with 2′-O,4′-C-aminomethylene bridge
```

(b)

```
Pyr15TM          5′-CTCTTCTTTTCTTTC-3′
Pyr15NC7-1       5′-CTCTTCTTTTCTTTC-3′
Pyr15NC7-2       5′-CTCTTCTTTTCTTTC-3′
Pyr15NC5-1       5′-CTCTTCTTTTCTTTC-3′
Pyr15NC5-2       5′-CTCTTCTTTTCTTTC-3′
Pur23A       5′-GCGCGAGAAGAAAAGAAAGCCGG-3′
Pyr23T       3′-CGCGCTCTTCTTTTCTTTCGGCC-5′
Pyr15NS2M        5′-TCTCTTCTTTTCTCT-3′
C: 5-methylcytosine
C: C with 2′-O,4′-C-aminomethylene bridge
T: T with 2′-O,4′-C-aminomethylene bridge
```

(c)

```
PCSK9-5-NC(T,C)  5′-d(GGTCCTCAGGGAACCAGGCC)-3′
(Target: 1287-1306 base of PCSK9 gene)
PCSK9-6-NC(T,C)  5′-d(GCCACCAGGTTGGGGGTCAG)-3′
(Target: 1315-1334 base of PCSK9 gene)
PCSK9-7-NC(T,C)  5′-d(CTGGAGCAGCTCAGCAGCTC)-3′
(Target: 1453-1472 base of PCSK9 gene)
PCSK9-8-NC(T,C)  5′-d(TAGACACCCTCACCCCCAAA)-3′
(Target: 1552-1571 base of PCSK9 gene)
PCSK9-10-NC(T,C) 5′-d(GCCGGCTCCGGCAGCAGATG)-3′
(Target: 2037-2056 base of PCSK9 gene)
C: 5-methylcytosine
C: C with 2′-O,4′-C-aminomethylene bridge
T: T with 2′-O,4′-C-aminomethylene bridge
```

(d)

Figure 1. a) Structural formulas for phosphodiester (PO) and 2′-*O*,4′-*C*-aminomethylene bridged nucleic acid (2′,4′-BNA^{NC})-modified backbones. (b) Oligonucleotide sequences for the unmodified (F12) or 2′,4′-BNA^{NC}-modified (F12-1, F12-31, F12-32, F12-6) oligonucleotide, the complementary RNA (R12R), the complementary single-mismatched RNA (R12X) and the complementary DNA (R12D) (c) Oligonucleotide sequences for the target duplex (Pur23APyr23T), the specific TFOs (Pyr15TM, Pyr15NC7-1, Pyr15NC7-2, Pyr15NC5-1, and Pyr15NC5-2), and the nonspecific oligonucleotide (Pyr15NS2M). (d) Oligonucleotide sequences for the 2′,4′-BNA^{NC}-modified antisense oligonucleotides to target a certain region of PCSK9 gene.

In this chapter, we describe the excellent properties of 2′,4′-BNA^{NC}-modified oligonucleotides for higher ability to form duplex and triplex and for higher nuclease resistance[11-13]. We also show the biological application of 2′,4′-BNA^{NC}-modified oligonucleotides to reduce expression level of target mRNA in mammalian cells[14]. PCSK9 is a serine protease involved in the degradation of LDL receptor [15-17]. Suppression of PCSK9 by reducing expression level of PCSK9 mRNA may cause an increase in the amount of the LDL receptor, resulting in the reduction of serum LDL cholesterol level. Thus, the PCSK9 mRNA has the potential to be an antisense target for the treatment of hypercholesterolemia [15-17]. We present the excellent antisense effect of 2′,4′-BNA^{NC} modified antisense oligonucleotides to reduce the expression level of the PCSK9 mRNA.

2. Methods to prepare and characterize oligonucleotides

2.1. Preparation of oligonucleotides

We synthesized complementary oligonucleotides for duplex DNA and unmodified homopyrimidine TFO (Figure 1b, 1c) on a DNA synthesizer using the solid-phase cyanoethyl phosphoramidite method, and purified them with a reverse-phase high performance liquid chromatography on a Wakosil DNA or Waters X-Terra column. 2′,4′-BNA^{NC}-modified oligonucleotides (Figure 1b, 1c, 1d) were synthesized and purified as described previously[10,11]. 5′-Biotinylated oligonucleotides were prepared from biotin phosphoramidite for kinetic analyses by Biacore described below. The concentration of all oligonucleotides was determined by UV absorbance. The reported extinction coefficient for poly (dT) [ε_{265} = 8700 cm^{-1} (mol of base/liter) $^{-1}$][18] was used for unmodified and 2′,4′-BNA^{NC}-modified homopyrimidine TFO. Complementary strands for duplex DNA were annealed by heating at up to 90 °C, followed by a gradual cooling to room temperature. When the removal of unpaired single strands is necessary, the annealed sample was applied on a hydroxyapatite column (BioRad). The concentration of duplex DNA was determined by UV absorbance, considering DNA concentration ratio of 1 OD = 50 μg/ml.

2.2. UV melting

Heating of duplex results in monophasic strand dissociation based on the transition between the two states, duplex→2 single strands. Heating of triplex also leads to biphasic strand dissociation according to the transitions between the three states, triplex→ duplex + single strand→3 single strands. Base stacking interactions in the free strands are weaker than those in the bound strands, resulting in a hyperchromic increase in UV absorbance upon heating. UV melting monitors the process of duplex and triplex melting by the temperature dependent change in UV absorbance. First derivative plot of UV absorbance (dA/dT vs T) is calculated from the UV melting curve (A vs T). Peak temperatures in the first derivative plot correspond to the melting temperature, T_m, of the transition.

UV melting experiments for duplex and triplex study were carried out on a DU-650 and DU-640 spectrophotometer (Beckman Inc.), respectively, equipped with a Peltier type cell holder. The cell path length was 1 cm. UV melting profiles for duplex study were measured in 10 mM sodium phosphate buffer at pH 7.2 containing 100 mM NaCl. UV melting profiles for triplex study were measured in 10 mM sodium cacodylate-cacodylic acid at pH 6.8 containing 200 mM NaCl and 20 mM $MgCl_2$. UV melting profiles were recorded at a scan rate of 0.5 °C/min with detection at 260 nm. The first derivative was calculated from the UV melting profile. The peak temperatures in the derivative curve were designated as the melting temperature, T_m. The duplex and triplex nucleic acid concentration used was 4 μM and 1 μM, respectively.

2.3. CD spectroscopy

CD spectroscopy is sensitive to interactions of nearby bases vertically stacked in strands. Stacking interactions depend on the conformational details of nucleic acid structure. CD spectra provide a certain basis for suggesting the overall conformation of strands in duplex and triplex. The appearance of an intense negative band at the short wavelength range (210-220 nm) in CD spectra indicates the formation of triplex.

CD spectra of the triplex at 20 °C were recorded in 10 mM sodium cacodylate-cacodylic acid at pH 6.8 containing 200 mM NaCl and 20 mM $MgCl_2$ on a JASCO J-720 spectropolarimeter interfaced with a microcomputer. The cell path length was 1 cm. The triplex nucleic acid concentration used was 1 μM.

2.4. Electrophoretic mobility shift assay (EMSA)

The ^{32}P-radiolabelled band of triplex migrates slower than that of duplex in native polyacrylamide gel electrophoresis. The formation of triplex results in appearance of a novel radiolabelled band shifted to a new position corresponding to triplex. The percentage of the formed triplex was calculated using the following equation:

$$\%_{\text{triplex}} = [S_{\text{triplex}} / (S_{\text{triplex}} + S_{\text{duplex}})] \times 100$$

where S_{triplex} and S_{duplex} represent the radioactive signal for triplex and duplex bands, respectively. The dissociation constant, K_d, of triplex formation is determined from the concentration of the TFO, which causes half of target duplex to shift to triplex.

EMSA experiments for the triplex formation were performed essentially as described previously by a 15% native polyacrylamide gel electrophoresis[12,13,19-27]. In a 9 μl of reaction mixture, ^{32}P-labeled Pur23A•Pyr23T duplex (~1 nM) (Figure 1c) was mixed with increasing concentrations of the specific TFO (Pyr15TM, Pyr15NC7-1, Pyr15NC7-2, Pyr15NC5-1, or Pyr15NC5-2) (Figure 1c) and the nonspecific oligonucleotide (Pyr15NS2M) (Figure 1c) in buffer [50 mM Tris-acetate (pH 7.0), 100 mM NaCl, and 10 mM $MgCl_2$]. Pyr15NS2M was added to achieve equimolar concentrations of TFO in each lane as well as to minimize adhesion of the DNA (duplex and TFO) to plastic surfaces during incubation

and subsequent losses during processing. After 6 h incubation at 37 °C, 2 μl of 50 % glycerol solution containing bromophenol blue was added without changing the pH and salt concentrations of the reaction mixtures. Samples were then directly loaded onto a 15 % native polyacrylamide gel prepared in buffer [50 mM Tris-acetate (pH 7.0) and 10 mM $MgCl_2$] and electrophoresis was performed at 8 V/cm for 16 h at 4 °C.

2.5. Thermodynamic analyses by isothermal titration calorimetry (ITC)

Isothermal titration calorimetry (ITC) relies upon the accurate measurement of heat changes caused by the interaction of molecules in solution and possesses the advantage of not requiring labeling or immobilization of the components[28]. ITC provides a great deal of thermodynamic information about the binding process from only a single experiment. This information includes the binding stoichiometry (n), the binding equilibrium constant (K_a), the enthalpy change (ΔH) of binding, the entropy change (ΔS) of binding and the Gibbs free energy change (ΔG) of the binding process[28]. A syringe containing a solution of one element (in the case of triplex formation, duplex) is incrementally titrated into a cell containing a solution of the second element (in the case of triplex formation, TFO). As the duplex is added to the TFO, heat is released upon the triplex formation. The heat for each injection is measured by the ITC instrument and is plotted as a function of time over the injection series. The heat signal from each injection is determined by the area underneath the injection peak. The heat is plotted against the molar ratio of the duplex added to the TFO added to the duplex in the cell. The titration plot provides the thermodynamic information of the triplex formation.

Isothermal titration experiments for the triplex formation were carried out on a VP ITC system (Microcal Inc., U.S.A.), essentially as described previously[12,13,19-22,25-27]. The TFO (Figure 1c) and Pur23A•Pyr23T duplex (Figure 1c) solutions were prepared by extensive dialysis against 10 mM sodium cacodylate-cacodylic acid at pH 6.1 or pH 6.8 containing 200 mM NaCl and 20 mM $MgCl_2$. The Pur23A•Pyr23T duplex solution in 10 mM sodium cacodylate-cacodylic acid at pH 6.1 or pH 6.8 containing 200 mM NaCl and 20 mM $MgCl_2$ was injected 20-times in 5-μl increments and 10-min intervals into the TFO solution without changing the reaction conditions. The heat for each injection was subtracted by the heat of dilution of the injectant, which was measured by injecting the Pur23A•Pyr23T duplex solution into the same buffer. Each corrected heat was divided by the moles of the Pur23A•Pyr23T duplex solution injected, and analyzed with Microcal Origin software supplied by the manufacturer.

2.6. Kinetic analyses by Biacore

Biacore is one example of a class of optical biosensors which can be used to determine the kinetic binding parameters of molecular interactions, such as association rate constant (k_{assoc}), dissociation rate constant (k_{dissoc}) and binding constant (K_a)[29,30]. Biacore measurements are usually performed with one partner immobilized (in the case of triplex

formation, duplex) on a porous hydrogel to which the second component (in the case of triplex formation, TFO) then binds[29]. Changes in the mass loading at the sensor surface upon the triplex formation cause a shift in the resonance angle of light propagated through the wave-guiding structure immediately adjacent to the hydrogel. The time dependence of the change in resonance angle yields the kinetic information of the triplex formation.

Kinetic experiments for the triplex formation were performed on a BIACORE J instrument (GE Healthcare, U.S.A.), in which a real-time biomolecular interaction was measured with a laser biosensor, essentially as described previously[12,13,19-25,27]. The layer of a SA sensor tip with immobilized streptavidin was equilibrated with 10 mM sodium cacodylate-cacodylic acid at pH 6.8 containing 200 mM NaCl and 20 mM $MgCl_2$ at a flow rate of 30 μl/min. 40 μl of 50 mM NaOH containing 1 M NaCl was injected 3 times at a flow rate of 30 μl/min to reduce electrostatic repulsion from the surface. After equilibrating with 10 mM sodium cacodylate-cacodylic acid at pH 6.8 containing 200 mM NaCl and 20 mM $MgCl_2$, 160 μl of 0.2 μM Bt(biotinylated)-Pyr23T•Pur23A duplex (Figure 1c) solution was added at a flow rate of 30 μl/min to bind with the streptavidin on the surface. After extensive washing and equilibrating the Bt-Pyr23T•Pur23A-immobilized surface with 10 mM sodium cacodylate-cacodylic acid at pH 6.8 containing 200 mM NaCl and 20 mM $MgCl_2$, 70 μl of the TFO (Figure 1c) solution in 10 mM sodium cacodylate-cacodylic acid at pH 6.8 containing 200 mM NaCl and 20 mM $MgCl_2$ was injected over the immobilized Bt-Pyr23T•Pur23A duplex at a flow rate of 30 μl/min, and then the triplex formation was monitored for 2 min. This was followed by washing the sensor tip with 10 mM sodium cacodylate-cacodylic acid at pH 6.8 containing 200 mM NaCl and 20 mM $MgCl_2$, and the dissociation of the preformed triplex was monitored for an additional 2.5 min. Finally, 40 μl of 100 mM Tris-HCl (pH 8.0) for Pyr15TM (Figure 1c), or 40 μl of 10 mM NaOH (pH 12) for Pyr15NC7-1, Pyr15NC7-2, Pyr15NC5-1, and Pyr15NC5-2 (Figure 1c) was injected at a flow rate of 30 μl/min to completely break the Hoogsteen hydrogen bonding between the TFO and Pur23A, during which the Bt-Pyr23T•Pur23A duplex may be partially denatured. The Bt-Pyr23T•Pur23A duplex was regenerated by injecting 0.2 μM Pur23A. The resulting sensorgrams were analyzed with the BIA evaluation software supplied by the manufacturer to calculate the kinetic parameters.

2.7. Stability of oligonucleotides in human serum against nuclease degradation

Stability of oligonucleotides in human serum was examined by the following two procedures[12,13,26].

a. Analyses by native polyacrylamide gel electrophoresis

Oligonucleotide (Figure 1c) was 5′-end labeled with ^{32}P using [γ-^{32}P] ATP and T4 polynucleotide kinase by a standard procedure. 2 pmol ^{32}P-labeled oligonucleotide was incubated at 37 °C in 200 μl of human serum from human male AB plasma (Sigma-Aldrich Co., USA). Aliquots of 5 μl were removed after 10, 20, 40, 60, and 120 min of incubation, and mixed with 5 μl of stop solution (80 % formamide, 50 mM EDTA) to terminate the reactions. The samples were loaded on 15 % native polyacrylamide gels prepared in buffer [50 mM

Tris-acetate (pH 7.0), 100 mM $MgCl_2$], and electrophoresis was performed at 8 V/cm and 4 °C. The gels were scanned and analyzed by BAS system.

b. Analyses by anion-exchange HPLC

1 nmol oligonucleotide (Figure 1c) was incubated at 37 °C in 20 μl of 50 % human serum from human male AB plasma (Sigma-Aldrich Co., USA). After incubation for 20, 60 and 120 min, the samples were mixed with 13 μl of formamide to terminate the reactions, and stored at -80 °C until HPLC analyses. The samples were mixed with 400 μl of HPLC buffer [25 mM Tris-HCl (pH 7.0), 0.5 % CH_3CN], and analyzed by anion-exchange HPLC on JASCO LC-2000 Plus series with detection at 260 nm using a linear gradient of 0-0.5 M NH_4Cl in HPLC buffer over 45 min to resolve the products. The HPLC column used was TSK-GEL DNA-NPR (Tosoh, Japan). Under these conditions, peaks of all proteins from the human serum could be resolved from those of the intact and degraded TFO. Degradation data from the acquired chromatograms were processed using ChromNAV software as supplied by the manufacturer.

2.8. In vitro assay of PCSK9 gene expression in mouse hepatocyte cell line, NMuLi

Mouse hepatocyte cell line NMuLi (4.0×10^5 cells/ml) was cultivated in 6 well plates (2 ml/well) and incubated for 24 hr at 37 °C under 5 % CO_2. Antisense oligonucleotide to target a certain region of PCSK9 gene (Figure 1d), Lipofectamine 2000 (Invitrogen), and Opti-MEM (Invitrogen) were mixed. The final concentration of the antisense oligonucleotide in the mixture was adjusted to 1, 3, 10, 30 or 50 nM. After incubation of the mixture for 20 min at room temperature, the mixture was transfected into the cell line. Cell culture medium was exchanged into the new one at 4 hr after the transfection of the antisense oligonucleotide. Cells were collected at 20 hr after the exchange of the cell culture medium. The collected cells were homogenized by ISOGEN (Nippon Gene) to extract total RNA. Concentration of the extracted total RNA was measured by UV absorbance. Length of the extracted total RNA was analyzed by agarose gel electrophoresis. After adjusting the concentration of the total RNA to 4.0 μg/10 μl, we performed reverse transcription reaction using the total RNA to obtain 1st strand cDNA. Then, we carried out real-time PCR using the obtained cDNA to quantitate the expression levels of PCSK9 mRNA and control housekeeping GAPDH mRNA. We normalized the expression level of PCSK9 mRNA by that of control housekeeping GAPDH mRNA, because the antisense oligonucleotides did not affect the expression level of control housekeeping GAPDH mRNA. We examined the effect of the antisense oligonucleotides on the expression level of PCSK9 mRNA.

3. Stabilization of duplex by 2′,4′-BNA^{NC}-modification

Formation of stable duplexes with complementary single-stranded RNA (ssRNA) and single-stranded DNA (ssDNA) under physiological condition is essential for antisense and diagnostic applications. Thermal stability of duplexes formed between a 12-mer unmodified

(F12; Figure 1b) or 2′,4′-BNA^{NC}-modified (F12-1, F12-31, F12-32, F12-6; Figure 1b) oligonucleotide and each of its complementary 12-mer ssRNA (R12R; Figure 1b) and 12-mer ssDNA (R12D; Figure 1b) was examined at pH 7.2 by UV melting (Table 1). The T_m value of the duplex formed between the 12-mer oligonucleotide containing a single 2′,4′-BNA^{NC}-modification (F12-1) and the complementary 12-mer ssRNA (R12R) increased by 6 °C compared to that of the duplex formed between the 12-mer unmodified oligonucleotide (F12) and R12R. Further incremental increase in T_m was observed upon an increase in the number of 2′,4′-BNA^{NC}-modification (F12-31, F12-32, F12-6). The increase in T_m per 2′,4′-BNA^{NC}-modification (ΔT_m/modification) ranged from 5.3 to 6.3 °C. These results indicate that further 2′,4′-BNA^{NC}-modification of oligonucleotide should produce very stable duplex with complementary ssRNA. On the other hand, a single 2′,4′-BNA^{NC}-modification increased the T_m value of the duplex formed with complementary 12-mer ssDNA (R12D) by only 1 °C (F12:R12D vs. F12-1:R12D), indicating that stabilization of duplex by 2′,4′-BNA^{NC}-modification is highly complementary ssRNA-selective. Similar to the case of complementary ssRNA, T_m was further increased by increasing the number of 2′,4′-BNA^{NC}-modification (F12-31, F12-32, F12-6). ΔT_m/modification for complementary ssDNA (R12D) ranging from 1.0 to 3.8 °C was smaller than that for complementary ssRNA (R12R) ranging from 5.3 to 6.3 °C.

Oligonucleotide	R12R: 3′-r(CGCAAAAAACGA)-5′	R12D: 3′-d(CGCAAAAAACGA)-5′
F12: 5′-d(GCGTTTTTTGCT)-3′	45	50
F12-1: 5′-d(GCGTTTTTTGCT)-3′[a]	51(+6.0)	51(+1.0)
F12-31: 5′-d(GCGTTTTTTGCT)-3′[a]	64(+6.3)	55(+1.7)
F12-32: 5′-d(GCGTTTTTTGCT)-3′[a]	61(+5.3)	57(+2.3)
F12-6: 5′-d(GCGTTTTTTGCT)-3′[a]	83(+6.3)	73(+3.8)

[a]2′,4′-BNA^{NC}-modified positions are underlined.

Table 1. Melting temperatures of 4 μM duplexes formed between 12-base unmodified (F12) or 2′,4′-BNA^{NC}-modified (F12-1, F12-31, F12-32, F12-6) oligonucleotides and each of complementary single-stranded RNA (R12R) and single-stranded DNA (R12D) in 10 mM sodium phosphate buffer (pH 7.2) and 100 mM NaCl. The increase in melting temperature per 2′,4′-BNA^{NC}-modification (ΔT_m/modification) is shown in parentheses.

Because 2′,4′-BNA^{NC}-modified oligonucleotides (F12-1, F12-31, F12-32, F12-6) exhibited high binding affinity with complementary ssRNA (R12R) as described above, their ability to discriminate bases was evaluated using single-mismatched ssRNA strand (R12X; Figure 1b) (Table 2). Any mismatched base in the ssRNA strands (R12U, R12G, R12C) resulted in a substantial decrease in the T_m value of the duplexes formed with the 2′,4′-BNA^{NC}-modified

oligonucleotide (F12-1). The T_m values of the duplexes formed with the 2′,4′-BNA^{NC}-modified oligonucleotide (F12-1:R12U, F12-1:R12G, F12-1:R12C) having a T-U, T-G, and T-C mismatched base pair were lower than those of the corresponding perfectly matched duplex (F12-1:R12A) by -14, -5, -17 °C, respectively. The mismatched base pair discrimination profile of the 2′,4′-BNA^{NC}-modified oligonucleotide (F12-1) was similar to that of the unmodified oligonucleotide (F12). These results indicate that 2′,4′-BNA^{NC}-modified oligonucleotide not only exhibits high-affinity RNA selective binding, but is also highly selective in recognizing bases.

Oligonucleotide	R12X: 3′-r(CGCAAXAAACGA)-5′			
	X = A (matched)	X = U	X = G	X = C
F12: 5′-d(GCGTTTTTTGCT)-3′	45	33	42	30
F12-1: 5′-d(GCGTTTTTTGCT)-3′[a]	51	37	46	34

[a]2′,4′-BNA^{NC}-modified position is underlined.

Table 2. Melting temperatures of 4 μM duplexes formed between 12-base unmodified (F12) or 2′,4′-BNA^{NC}-modified (F12-1) oligonucleotides and complementary single-stranded RNA containing a single-mismatched base (R12X) in 10 mM sodium phosphate buffer (pH 7.2) and 100 mM NaCl.

4. Stabilization of pyrimidine motif triplex at neutral pH by 2′,4′-BNA^{NC}-modification

Formation of stable triplex with TFO under physiological condition is essential for antigene application. Thermal stability of the pyrimidine motif triplexes formed between a 23-bp target duplex (Pur23A•Pyr23T; Figure 1c) and each of its specific 15-mer 2′,4′-BNA^{NC}-unmodified (Pyr15TM; Figure 1c) or 2′,4′-BNA^{NC}-modified (Pyr15NC7-1, Pyr15NC7-2, Pyr15NC5-1, or Pyr15NC5-2; Figure 1c) TFO was investigated at pH 6.8 by UV melting (Figure 2 and Table 3). UV melting curves in the both directions (heating and cooling) are almost superimposable in all cases, indicating that the dissociation and association processes are reversible. The triplex involving Pyr15TM showed two-step melting. Upon heating the first transition at lower temperature, T_{m1} (39.1 °C), was the melting of the triplex to a duplex and a TFO, and the second transition at higher temperature, T_{m2} (72.4 °C), was the melting of the duplex (Figure 2). On the other hand, the triplex involving each of the 2′,4′-BNA^{NC}-modified TFOs showed only one transition at higher temperature, T_m. As the magnitude in UV absorbance change at T_m for each of the 2′,4′-BNA^{NC}-modified TFOs was almost equal to the sum of those at T_{m1} and T_{m2} for Pyr15TM (Figure 2), the transition was identified as a direct melting of the triplex to its constituting single-strand DNAs upon heating. The 2′,4′-BNA^{NC} modification, therefore, increased the melting temperature of the triplex by more than 35 °C (Table 3), indicating that the 2′,4′-BNA^{NC} modification of TFO increased the thermal stability of the pyrimidine motif triplex at neutral pH.

TFO	T_{m1} (°C)	T_{m2} (°C)
Pyr15TM	39.1 ± 0.1	72.4 ± 0.4
Pyr15BNANC7-1		79.4 ± 0.6
Pyr15BNANC7-2		85.8 ± 0.1
Pyr15BNANC5-1		75.6 ± 0.7
Pyr15BNANC5-2		75.6 ± 0.7

Table 3. Melting temperatures of the triplexes between a 23-base pair target duplex (Pur23A•Pyr23T) and a 15-mer TFO (Pyr15TM, Pyr15BNANC7-1, Pyr15BNANC7-2, Pyr15BNANC5-1, or Pyr15BNANC5-2) in 10 mM sodium cacodylate-cacodylic acid (pH 6.8), 200 mM NaCl and 20 mM $MgCl_2$.

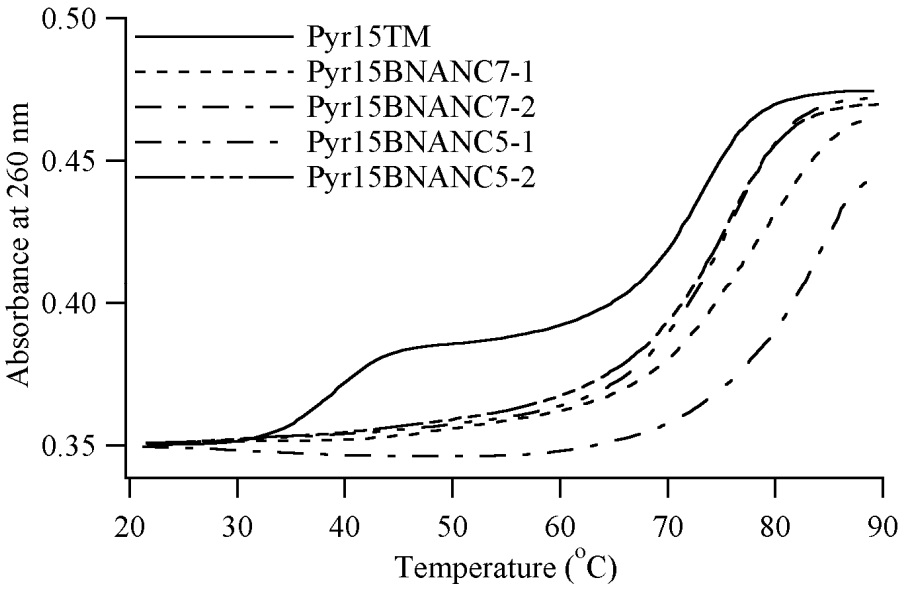

Figure 2. . UV melting profiles of the pyrimidine motif triplex with the specific TFO (Pyr15TM, Pyr15NC7-1, Pyr15NC7-2, Pyr15NC5-1, or Pyr15NC5-2) upon heating. The triplexes with Pyr15TM, Pyr15NC7-1, Pyr15NC7-2, Pyr15NC5-1, or Pyr15NC5-2 in 10 mM sodium cacodylate-cacodylic acid (pH 6.8), 200 mM NaCl and 20 mM $MgCl_2$ were melted at a scan rate of 0.5 °C/min with detection at 260 nm. The cell path length was 1 cm. The triplex nucleic acid concentration used was 1 μM.

5. No significant structural change of pyrimidine motif triplex at neutral pH by 2′,4′-BNA^{NC}-modification

Circular dichroism (CD) spectra of the pyrimidine motif triplexes between the target duplex (Pur23A•Pyr23T) and each of the 2′,4′-BNA^{NC}-unmodified (Pyr15TM) or 2′,4′-BNA^{NC}-modified (Pyr15NC7-1, Pyr15NC7-2, Pyr15NC5-1, or Pyr15NC5-2) TFO were measured at 20 °C and pH 6.8 (Figure 3). A significant negative band in the short-wavelength (210-220 nm) region was observed for all the profiles (Figure 3), confirming the triplex formation involving each TFO[31]. The overall shape of the CD spectra was quite similar among all the profiles (Figure 3), suggesting that no significant change may be induced in the higher order structure of the pyrimidine motif triplex by the 2′,4′-BNA^{NC} modification.

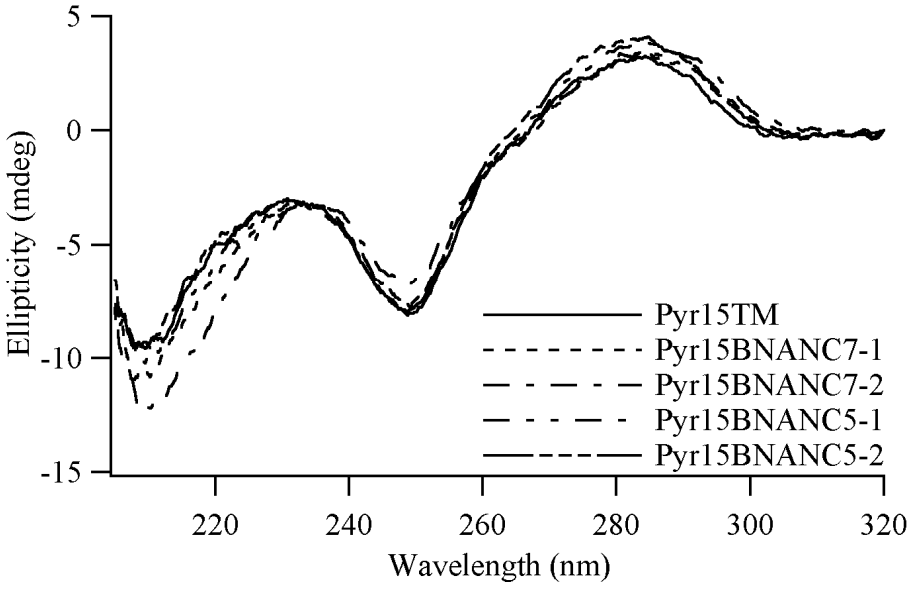

Figure 3. CD spectra of the pyrimidine motif triplex with the specific TFO (Pyr15TM, Pyr15NC7-1, Pyr15NC7-2, Pyr15NC5-1, or Pyr15NC5-2). The triplexes with Pyr15TM, Pyr15NC7-1, Pyr15NC7-2, Pyr15NC5-1, or Pyr15NC5-2 in 10 mM sodium cacodylate-cacodylic acid (pH 6.8), 200 mM NaCl and 20 mM $MgCl_2$ were measured at 20 °C in the wavelength range of 205-320 nm. The cell path length was 1 cm. The triplex nucleic acid concentration used was 1 μM.

6. Promotion of pyrimidine motif triplex formation at neutral pH by 2′,4′-BNA^{NC}-modification

The pyrimidine motif triplex formation between the target duplex (Pur23A•Pyr23T) and each of the 2′,4′-BNA^{NC}-unmodified (Pyr15TM) or 2′,4′-BNA^{NC}-modified (Pyr15NC7-1, Pyr15NC7-2, Pyr15NC5-1, or Pyr15NC5-2) TFO was examined at pH 7.0 by EMSA (Figure

4). Total oligonucleotide concentration ([specific TFO (Pyr15TM or 2′,4′-BNA^{NC}-modified TFO)] + [nonspecific oligonucleotide (Pyr15NS2M)]) was kept constant at 1000 nM to minimize loss of DNA during processing and to assess sequence specificity. While incubation with 1000 nM Pyr15NS2M alone did not cause a shift in electrophoretic migration of the target duplex (see *lane 1* for Pyr15TM), those with Pyr15TM or each of the 2′,4′-BNA^{NC}-modified TFOs at particular concentrations caused retardation of the duplex migration owing to triplex formation[32]. The dissociation constant, K_d, of triplex formation was determined from the concentration of the TFO, which caused half of the target duplex to shift to the triplex[32]. The K_d of the triplex with Pyr15TM was estimated to be between 250 and 1000 nM. In contrast, the K_d of the triplex with each of the 2′,4′-BNA^{NC}-modified TFOs was ~16 nM, indicating that the 2′,4′-BNA^{NC} modification of TFO increased the binding constant, K_a (= $1/K_d$), of the pyrimidine motif triplex formation at neutral pH by more than 10-fold. The increase in the K_a by the 2′,4′-BNA^{NC} modification of TFO was similar in magnitude among the four modified TFOs.

7. Thermodynamic analyses of pyrimidine motif triplex formation involving 2′,4′-BNA^{NC}-modified TFO at neutral pH

We examined the thermodynamic parameters of the pyrimidine motif triplex formation between the target duplex (Pur23A•Pyr23T) and each of the 2′,4′-BNA^{NC}-unmodified (Pyr15TM) or 2′,4′-BNA^{NC}-modified TFO at 25 °C and pH 6.8 by ITC. To investigate the pH dependence of the pyrimidine motif triplex formation, the thermodynamic parameters of the triplex formation between Pur23A•Pyr23T and Pyr15TM were also analyzed at 25 °C and pH 6.1 by ITC. Figure 5a shows a typical ITC profile for the triplex formation between Pyr15NC7-1 and Pur23A•Pyr23T at 25 °C and pH 6.8. An exothermic heat pulse was observed after each injection of Pur23A•Pyr23T into Pyr15NC7-1. The magnitude of each peak decreased gradually with each new injection, and a small peak was still observed at a molar ratio of [Pur23A•Pyr23T]/[Pyr15NC7-1]=2. The area of the small peak was equal to the heat of dilution measured in a separate experiment by injecting Pur23A•Pyr23T into the same buffer. The area under each peak was integrated, and the heat of dilution of Pur23A•Pyr23T was subtracted from the integrated values. The corrected heat was divided by the moles of injected solution, and the resulting values were plotted as a function of a molar ratio of [Pur23A•Pyr23T]/[Pyr15NC7-1], as shown in Figure 5b. The resultant titration plot was fitted to a sigmoidal curve by a nonlinear least-squares method. The binding constant, K_a, and the enthalpy change, ΔH, were obtained from the fitted curve[28]. The Gibbs free energy change, ΔG, and the entropy change, ΔS, were calculated from the equation, $\Delta G = -RT\ln K_a = \Delta H - T\Delta S$, where R is gas constant and T is temperature[28]. The titration plots for Pyr15TM at pH 6.8 and pH 6.1 are also shown in Figure 5b. The thermodynamic parameters for Pyr15TM at pH 6.8 and pH 6.1 were obtained from the titration plots in the same way. The ITC profiles and the titration plots for each of other 2′,4′-BNA^{NC}-modified TFOs at pH 6.8 were almost the same as those observed for Pyr15NC7-1 at pH 6.8. The thermodynamic parameters for each of other 2′,4′-BNA^{NC}-modified TFOs at pH 6.8 were obtained from the titration plots in the same way.

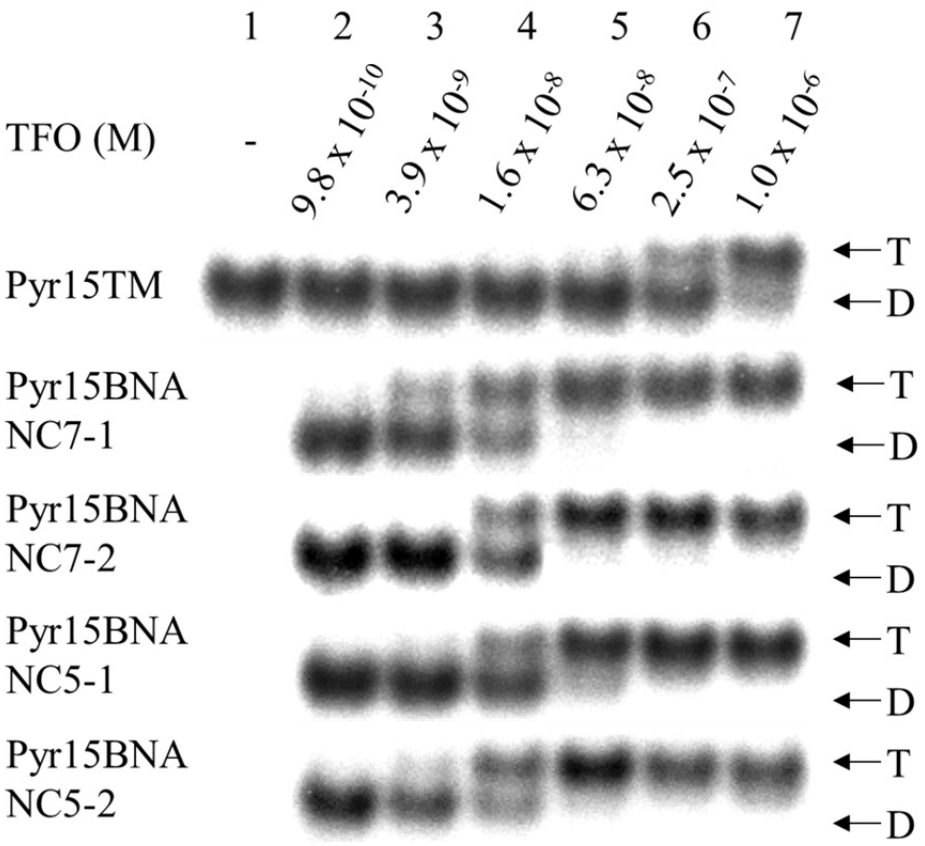

Figure 4. EMSA of the pyrimidine motif triplex formation with the specific TFO (Pyr15TM, Pyr15NC7-1, Pyr15NC7-2, Pyr15NC5-1, or Pyr15NC5-2) at neutral pH. Triplex formation was initiated by adding ^{32}P-labeled Pur23APyr23T duplex (~1 nM) with the indicated final concentrations of the specific TFO (Pyr15TM, Pyr15NC7-1, Pyr15NC7-2, Pyr15NC5-1, or Pyr15NC5-2). The nonspecific oligonucleotide (Pyr15NS2M) was added to adjust the equimolar concentrations (1000 nM) of TFO (Pyr15TM+Pyr15NS2M, Pyr15NC7-1+Pyr15NS2M, Pyr15NC7-2+Pyr15NS2M, Pyr15NC5-1+Pyr15NS2M, or Pyr15NC5-2+Pyr15NS2M) in each lane. Reaction mixtures involving Pyr15TM, Pyr15NC7-1, Pyr15NC7-2, Pyr15NC5-1, or Pyr15NC5-2 in 50 mM Tris-acetate (pH 7.0), 100 mM NaCl, and 10 mM $MgCl_2$ were incubated for 6 h at 37 ^{o}C, and then electrophoretically separated at 4 ^{o}C on a 15 % native polyacrylamide gel prepared in buffer [50 mM Tris-acetate (pH 7.0) and 10 mM $MgCl_2$]. Positions of the duplex (D) and triplex (T) are indicated.

Table 4 summarizes the thermodynamic parameters for the pyrimidine motif triplex formation with each of Pyr15TM and the 2′,4′-BNA^{NC}-modified TFOs at 25 °C and pH 6.8, and those with Pyr15TM at 25 °C and pH 6.1, obtained from ITC. The signs of both ΔH and ΔS were negative under each condition. Because an observed negative ΔS was unfavorable for the triplex formation, the triplex formation was driven by a large negative ΔH under each condition. The K_a for Pyr15TM at pH 6.1 was ~10-fold larger than that observed for Pyr15TM at pH 6.8, confirming, like others[5-7], that neutral pH is unfavorable for the pyrimidine motif triplex formation involving C$^+$•G:C triads. In addition, the K_a for each of the 2′,4′-BNA^{NC}-modified TFOs at pH 6.8 was ~10-fold larger than that observed for Pyr15TM at pH 6.8 (Table 4), indicating that the 2′,4′-BNA^{NC} modification of TFO increased the K_a for the pyrimidine motif triplex formation at neutral pH, which is consistent with the results of EMSA (Figure 4). The increase in the K_a by the 2′,4′-BNA^{NC} modification of TFO was similar in magnitude among the four 2′,4′-BNA^{NC}-modified TFOs. Also, although the K_a and ΔG for the triplex formation with each of the 2′,4′-BNA^{NC}-modified TFOs at pH 6.8 and those with Pyr15TM at pH 6.1 were quite similar, the constituents of ΔG, that is, ΔH and ΔS, were obviously different from each other (Table 4). The magnitudes of the negative ΔH and ΔS for each of the 2′,4′-BNA^{NC}-modified TFOs at pH 6.8 were significantly smaller than those observed for Pyr15TM at pH 6.1 (Table 4).

TFO	pH	K_a (M^{-1})	K_a (relative)	ΔG (kcal mol^{-1})	ΔH (kcal mol^{-1})	ΔS (cal mol^{-1} K^{-1})
Pyr15TM	6.1[a]	(5.81 ± 0.99) x 10^6	13.9	-9.23 ± 0.11	-92.0 ± 1.5	-278 ± 5
Pyr15TM	6.8[b]	(4.19 ± 2.0) x 10^5	1.0	-7.67 ± 0.38	-38.5 ± 7.5	-103 ± 26
Pyr15BNANC7-1	6.8[b]	(5.30 ± 0.45) x 10^6	12.6	-9.17 ± 0.05	-56.1 ± 1.0	-157 ± 4
Pyr15BNANC7-2	6.8[b]	(4.10 ± 0.69) x 10^6	9.8	-9.02 ± 0.11	-62.1 ± 2.4	-178 ± 8
Pyr15BNANC5-1	6.8[b]	(3.73 ± 0.43) x 10^6	8.9	-8.96 ± 0.07	-54.3 ± 1.5	-152 ± 5
Pyr15BNANC5-2	6.8[b]	(3.82 ± 0.29) x 10^6	9.1	-8.98 ± 0.05	-53.8 ± 1.1	-150 ± 4

[a]10 mM sodium cacodylate-cacodylic acid (pH 6.1), 200 mM NaCl and 20 mM $MgCl_2$. [b]10 mM sodium cacodylate-cacodylic acid (pH 6.8), 200 mM NaCl and 20 mM $MgCl_2$.

Table 4. Thermodynamic parameters for the triplex formation between a 23-base pair target duplex (Pur23A•Pyr23T) and a 15-mer TFO (Pyr15TM, Pyr15BNANC7-1, Pyr15BNANC7-2, Pyr15BNANC5-1, or Pyr15BNANC5-2) at 25 °C, obtained from ITC

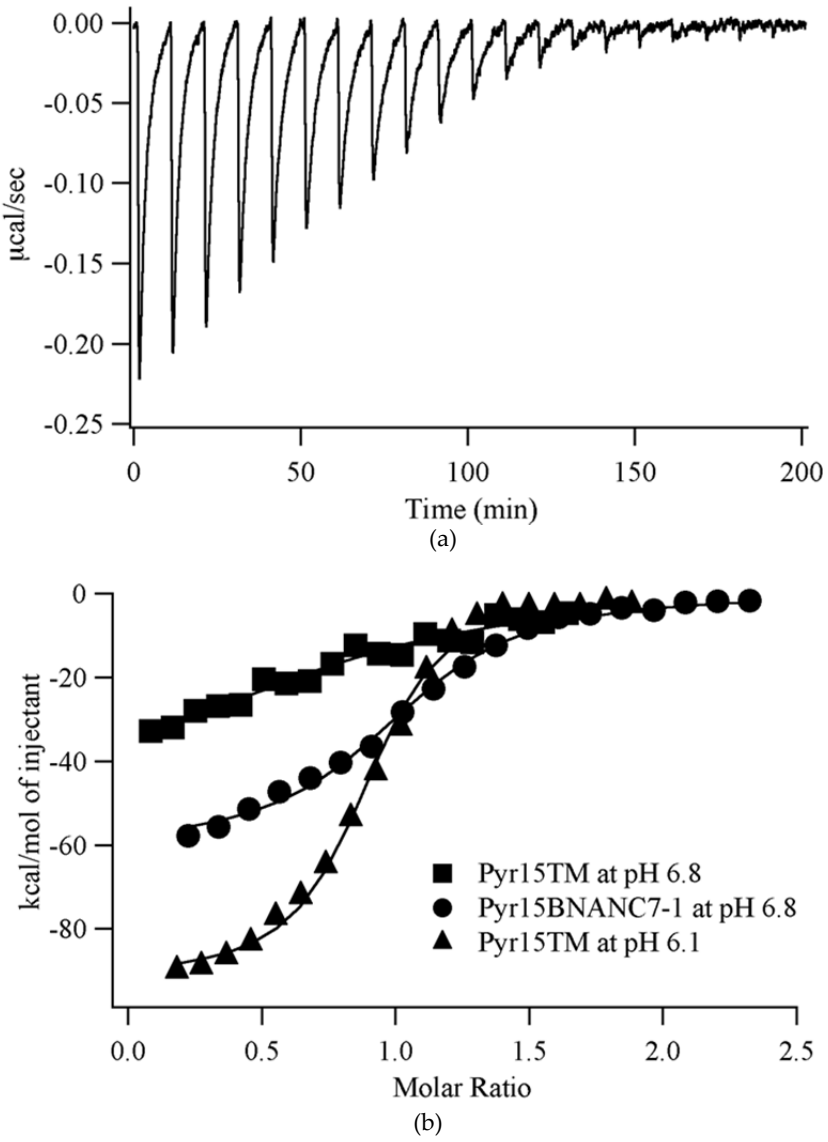

Figure 5. Thermodynamic analyses of the pyrimidine motif triplex formation with Pyr15TM or Pyr15NC7-1 at pH 6.8 and with Pyr15TM at pH 6.1 by ITC. (a) Typical ITC profiles for the triplex formation between Pyr15NC7-1 and Pur23APyr23T at 25 °C and pH 6.8. 114.7 μM Pur23APyr23T solution in 10 mM sodium cacodylate-cacodylic acid (pH 6.8), 200 mM NaCl and 20 mM $MgCl_2$ was injected 20 times in 5-μl increments into 3.58 μM Pyr15NC7-1 solution, which was dialyzed against the same buffer. Injections were occurred over 12 s at 10-min intervals. (b) The titration plots against the molar ratio of [Pur23APyr23T]/ [TFO]. The data were fitted by a nonlinear least-squares method.

8. Kinetic analyses of pyrimidine motif triplex formation involving 2′,4′-BNA^{NC}-modified TFO at neutral pH

To examine the putative mechanism involved in the increase in K_a of the pyrimidine motif triplex formation by the 2′,4′-BNA^{NC} modification of TFO (Figure 4 and Table 4), we assessed the kinetic parameters for the association and dissociation of TFO (Pyr15TM and the 2′,4′-BNA^{NC}-modified TFOs) with Pur23A•Pyr23T at 25 °C and pH 6.8 by BIACORE. Figure 6a shows the sensorgrams representing the triplex formation and dissociation involving the various concentrations of Pyr15NC7-1. The injection of Pyr15NC7-1 over the immobilized Bt(biotinylated)-Pyr23T•Pur23A caused an increase in response. As shown in Figure 6a, an increase in the concentration of Pyr15NC7-1 led to a gradual change in the response of the association curves. The on-rate constant (k_{on}) was obtained from the analysis of each association curve. Figure 6b shows a plot of k_{on} against the Pyr15NC7-1 concentrations. The resultant plot was fitted to a straight line by a linear least-squares method. The association rate constant (k_{assoc}) was determined from the slope of the fitted line[29,30]. The off-rate constant (k_{off}) was obtained from the analysis of each dissociation curve (Figure 6a). As k_{off} is usually independent of the concentration of the injected solution, the dissociation rate constant (k_{dissoc}) was determined by averaging k_{off} for several concentrations[29,30]. K_a was calculated from the equation, $K_a = k_{assoc}/k_{dissoc}$. The kinetic parameters for each of Pyr15TM and other 2′,4′-BNA^{NC}-modified TFOs were obtained in the same way.

TFO	k_{assoc} (M^{-1} s^{-1})	k_{assoc} (relative)	k_{dissoc} (s^{-1})	k_{dissoc} (relative)	K_a (M^{-1})	K_a (relative)
Pyr15TM	(2.01 ± 0.11) x 10^2	1.0	(1.05 ± 0.29) x 10^{-3}	1.0	(1.91 ± 0.88) x 10^5	1.0
Pyr15BNANC7-1	(3.81 ± 0.60) x 10^2	1.9	(6.96 ± 1.14) x 10^{-5}	0.066	(5.47 ± 2.10) x 10^6	28.6
Pyr15BNANC7-2	(4.61 ± 0.29) x 10^2	2.3	(7.99 ± 0.83) x 10^{-5}	0.076	(5.77 ± 1.07) x 10^6	30.2
Pyr15BNANC5-1	(4.60 ± 0.18) x 10^2	2.3	(9.36 ± 1.29) x 10^{-5}	0.089	(4.91 ± 1.01) x 10^6	25.7
Pyr15BNANC5-2	(4.30 ± 0.67) x 10^2	2.1	(6.61 ± 0.81) x 10^{-5}	0.063	(6.51 ± 2.06) x 10^6	34.1

Table 5. Kinetic parameters for the triplex formation between a 23-base pair target duplex (Pur23A•Pyr23T) and a 15-mer TFO (Pyr15TM, Pyr15BNANC7-1, Pyr15BNANC7-2, Pyr15BNANC5-1, or Pyr15BNANC5-2) at 25 °C and pH 6.8 in 10 mM sodium cacodylate-cacodylic acid, 200 mM NaCl and 20 mM $MgCl_2$, obtained from BIACORE interaction analysis system

Table 5 summarizes the kinetic parameters for the pyrimidine motif triplex formation with each of Pyr15TM and the 2′,4′-BNA^{NC}-modified TFOs at 25 °C and pH 6.8, obtained from BIACORE. The magnitudes of K_a calculated from the ratio of k_{assoc} to k_{dissoc} (Table 5) were consistent with those obtained from ITC (Table 4). The K_a for each of the 2′,4′-BNA^{NC}-modified TFOs at pH 6.8 was ~30-fold larger than that observed for Pyr15TM at pH 6.8, indicating that the 2′,4′-BNA^{NC} modification of TFO increased the K_a of the pyrimidine motif triplex formation at neutral pH, which supported the results of EMSA (Figure 4) and ITC (Table 4). The 2′,4′-BNA^{NC} modification of TFO decreased k_{dissoc} by ~15-fold, while it

moderately increased k_{assoc} by ~2-fold. Thus, the much larger K_a by the 2′,4′-BNA^{NC} modification of TFO resulted mainly from the decrease in k_{dissoc} rather than the increase in $k_{assoc.}$

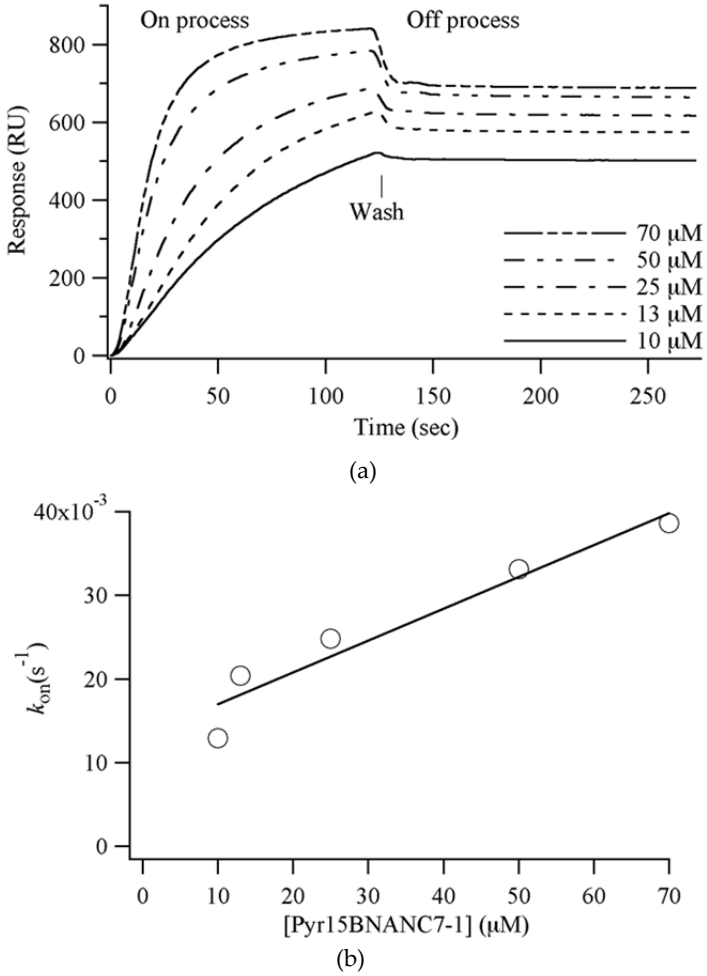

Figure 6. Kinetic analyses of the pyrimidine motif triplex formation with Pyr15NC7-1 in 10 mM sodium cacodylate-cacodylic acid (pH 6.8), 200 mM NaCl and 20 mM $MgCl_2$ by BIACORE interaction analysis system. (a) A series of sensorgrams for the triplex formation and the dissociation of the formed triplex between Pyr15NC7-1 and Pur23APyr23T at 25 °C and pH 6.8. The Pyr15NC7- 1 solutions, diluted in the buffer to achieve the indicated final concentrations, were injected into the Bt-Pyr23TPur23A-immobilized cuvette. The binding of Pyr15NC7-1 to Bt-Pyr23TPur23A and the dissociation of Pyr15NC7-1 from Bt-Pyr23TPur23A were monitored as the response against time. (b) Measured on-rate constants, k_{on}, of the triplex formation in (a) were plotted against the respective concentrations of Pyr15NC7-1. The plot was fitted to a straight line ($r^2 = 0.97$) by a linear least-squares method.

9. Increased stability of 2′,4′-BNA^{NC}-modified oligonucleotides in human serum against nuclease degradation

A major difficulty associated with the use of oligonucleotides as *in vivo* agents is the rapid degradation of oligonucleotides by nuclease *in vivo*[8]. To propose the possibility for the application of 2′,4′-BNA^{NC}-modified oligonucleotides to the various strategies *in vivo*, we examined the resistance of the 2′,4′-BNA^{NC}-unmodified (Pyr15TM) or 2′,4′-BNA^{NC}-modified oligonucleotides against nuclease degradation in human serum. The series of oligonucleotides 5′-end labeled with ^{32}P were incubated at 37 ^{o}C in human serum, and their degradation was assessed by 15 % native polyacrylamide gel electrophoresis (Figure 7). All of Pyr15TM was degraded and converted to shorter oligonucleotides within 20 min of incubation. In contrast, no significant degradation of Pyr15NC7-2 and Pyr15NC5-2 was observed even after 120 min of incubation. These results indicate that the 2′,4′-BNA^{NC} modification contributed to increase the stability of TFOs in human serum. Because Pyr15NC7-1 and Pyr15NC5-1 containing the 2′,4′-BNA^{NC} modification at the 5′-end were unable to be labeled with ^{32}P by T4 polynucleotide kinase, the stability of Pyr15NC7-1 and Pyr15NC5-1 in human serum was impossible to be examined. Thus, to investigate the resistance of all TFOs including Pyr15NC7-1 and Pyr15NC5-1 against nuclease degradation, their degradation was estimated by anion-exchange HPLC after incubating the TFOs at 37 ^{o}C in human serum. Figure 8 shows the percentage of the intact oligonucleotides as a function of the incubation time. Only 20 % of intact Pyr15TM was detected after 20 min of incubation with human serum, and Pyr15TM was completely degraded within 60 min. On the other hand, more than 50 % of the 2′,4′-BNA^{NC}-modified TFOs remained intact even after 120 min of incubation with human serum. These results indicate that the 2′,4′-BNA^{NC} modification significantly increased the nuclease resistance of TFOs in human serum. The results of anion-exchange HPLC are consistent with those of native polyacrylamide gel electrophoresis (Figure 7).

10. Excellent antisense effect of 2′,4′-BNA^{NC}-modified antisense oligonucleotides on the expression level of PCSK9 mRNA

We examined *in vitro* antisense effect of 2′,4′-BNA^{NC}-modified antisense oligonucleotides (Figure 1d) on the expression level of PCSK9 mRNA. A series of the concentrations of 2′,4′-BNA^{NC}-modified antisense oligonucleotides were transfected into mouse hepatocyte cell line, NMuLi, by lipofectamine 2000. Total RNA was extracted from the cells at 24 hr after the transfection. The expression level of PCSK9 mRNA was quantitated by real-time RT-PCR relative to that of control housekeeping GAPDH mRNA. In all cases of the 2′,4′-BNA^{NC}-modified antisense oligonucleotides, the expression level of PCSK9 mRNA was decreased upon increasing the concentration of the 2′,4′-BNA^{NC}-modified antisense oligonucleotides (Figure 9). The 2′,4′-BNA^{NC}-modified antisense oligonucleotides showed the excellent antisense effect to reduce the expression level of PCSK9 mRNA.

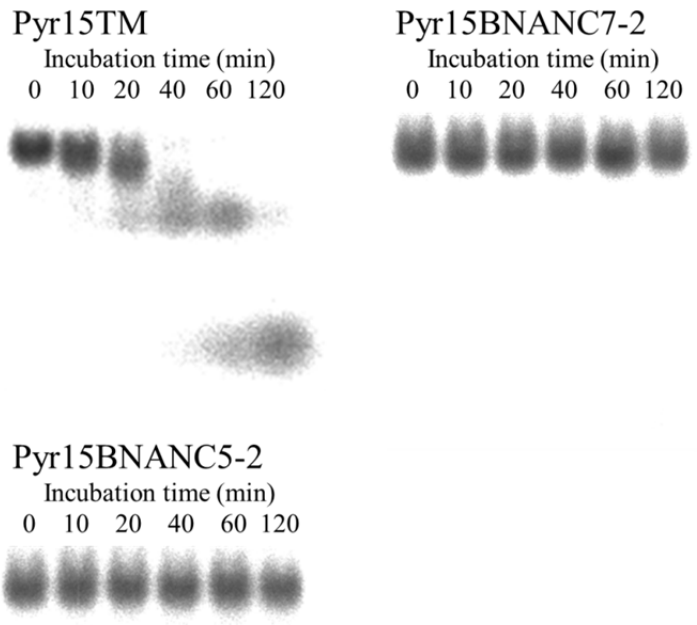

Figure 7. Stability of the specific TFOs (Pyr15TM, Pyr15BNANC7-2, and Pyr15BNANC5-2) in human serum. 2 pmol ^{32}P-labeled TFOs were incubated in human serum at 37°C, and aliquots were removed at the time points indicated and analyzed by 15 % native polyacrylamide gel electrophoresis.

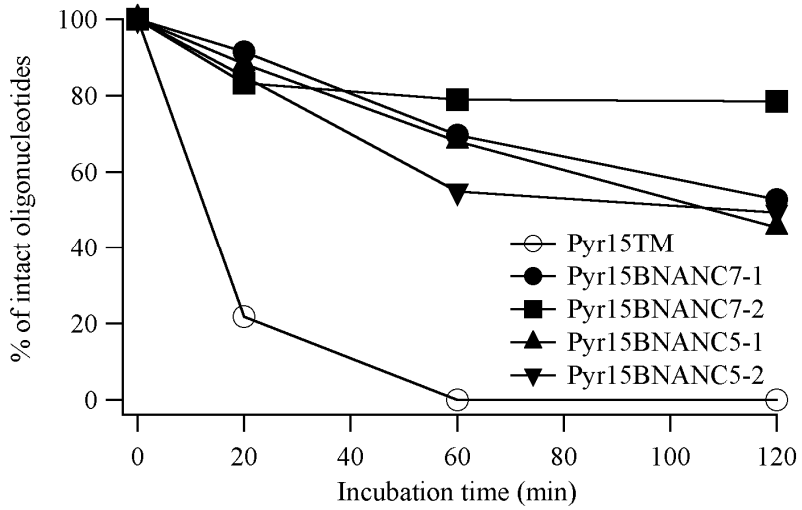

Figure 8. Stability of the specific TFOs (Pyr15TM, Pyr15NC7-1, Pyr15NC7-2, Pyr15NC5-1, and Pyr15NC5-2) in human serum. 1 nmol TFOs were incubated in human serum at 37 °C, and aliquots were removed at the time points indicated and analyzed by anion-exchange HPLC. The percentage of the intact oligonucleotides was determined and plotted as a function of the incubation time.

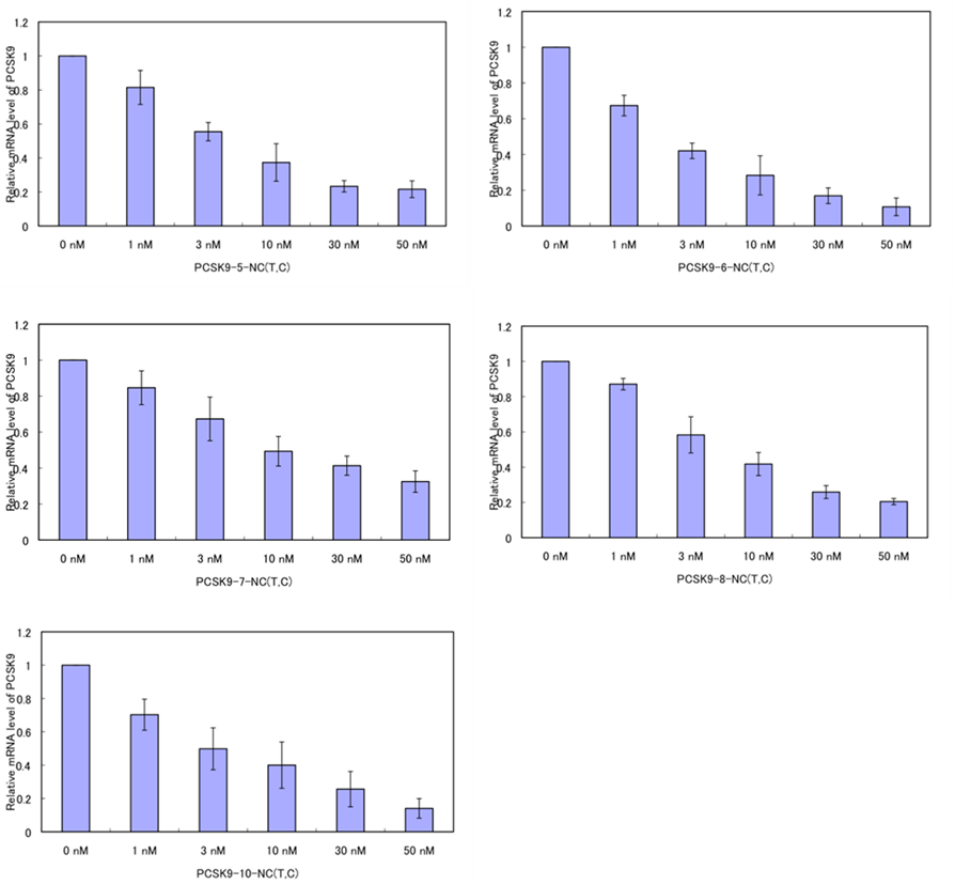

Figure 9. Relative expression level of PCSK9 mRNA as a function of the concentrations of 2′,4′-BNA^{NC}-modified antisense oligonucleotide. The expression level of PCSK9 mRNA was quantitated by real-time RT-PCR relative to that of control housekeeping GAPDH mRNA. The expression level of PCSK9 mRNA with the addition of 2′,4′-BNA^{NC}-modified antisense oligonucleotide was divided by that without the addition of the antisense oligonucleotide to obtain relative expression level of PCSK9 mRNA.

11. Discussion

The T_m value of the duplex formed between the 2′,4′-BNA^{NC}-modified oligonucleotide and the complementary ssRNA or ssDNA was significantly higher than that of the duplex formed between the corresponding unmodified oligonucleotide and the same complementary ssRNA or ssDNA (Table 1). The ΔT_m/modification value for the complementary ssRNA was significantly larger than that for the corresponding complementary ssDNA (Table 1), indicating that the 2′,4′-BNA^{NC}-modified oligonucleotide selectively bound to the complementary ssRNA with high affinity. In addition, the 2′,4′-BNA^{NC}-modified oligonucleotide recognized the base in the complementary strand with

high selectivity (Table 2). These results indicate that the 2′,4′-BNA^{NC}-modification of oligonucleotide promotes the duplex formation involving the complementary ssRNA with high sequence selectivity at neutral pH.

The K_a of the pyrimidine motif triplex formation with Pyr15TM at pH 6.1 was ~10-fold larger than that observed with Pyr15TM at pH 6.8 (Table 4), which is consistent with the previously reported results that neutral pH is unfavorable for the pyrimidine motif triplex formation involving C$^+$·G:C triads[5-7]. On the other hand, the K_a of the pyrimidine motif triplex formation with each of the 2′,4′-BNA^{NC}-modified TFOs at pH 6.8 was ~10-fold larger than that observed with Pyr15TM at pH 6.8 (Table 4). The increase in K_a at neutral pH by the 2′,4′-BNA^{NC} modification of TFO was supported by the results of EMSA (Figure 4) and BIACORE (Table 5), although the magnitudes of K_d (=1/K_a) were different between EMSA (Figure 4) and each of ITC (Table 4) or BIACORE (Table 5) due to the difference in the experimental buffer conditions. In addition, the 2′,4′-BNA^{NC} modification of TFO increased the thermal stability of the pyrimidine motif triplex at neutral pH (Figure 2 and Table 3). These results indicate that the 2′,4′-BNA^{NC} modification of TFO promotes the pyrimidine motif triplex formation at neutral pH.

Because the formed triplex structure involving Pyr15TM at pH 6.1 and that involving Pyr15TM at pH 6.8 are the same, the magnitude of ΔH and ΔS upon the triplex formation measured by ITC could be the same between the two conditions. However, the magnitudes of ΔH and ΔS for Pyr15TM at pH 6.8 were significantly smaller than those observed for Pyr15TM at pH 6.1 (Table 4). When the ΔH and ΔS are calculated from the fitting procedure of ITC, the heat observed by ITC is divided not by the effective concentration really involved in the triplex formation, but by the apparent concentration added to the triplex formation[28]. The calculation does not take it into consideration how many percentage of the added concentration is really effectively involved in the triplex formation. Thus, if the triplex formation is substoichiometric under a certain condition, the magnitudes of ΔH and ΔS for the substoichiometric triplex formation estimated by ITC should be smaller than those observed for the more stoichiometric triplex formation under another condition. Therefore, the significantly smaller magnitudes of ΔH and ΔS for Pyr15TM at pH 6.8 relative to those for Pyr15TM at pH 6.1 (Table 4) suggest that the triplex formation with Pyr15TM at pH 6.8 was significantly more substoichiometric than that with Pyr15TM at pH 6.1, which was also supported by the significantly smaller magnitudes of K_a and ΔG for Pyr15TM at pH 6.8 (Table 4). In the substoichiometric triplex formation, the cytosine bases in the TFO may be protonated to a lesser extent, resulting in weaker hydrogen bonding interactions and possibly also weaker base stacking interactions. In contrast, the K_a and ΔG for Pyr15TM at pH 6.1 and those for the 2′,4′-BNA^{NC}-modified TFOs at pH 6.8 were quite similar (Table 4), suggesting that the triplex formations under these conditions were similarly quite stoichiometric. Thus, to discuss the promotion mechanism of the triplex formation by the 2′,4′-BNA^{NC} modification of TFO, the comparison of the ΔH and ΔS between Pyr15TM at pH 6.8 and the 2′,4′-BNA^{NC}-modified TFOs at pH 6.8 is not valid due to the significant substoichiometry for Pyr15TM at pH 6.8. The comparison of the ΔH and ΔS between Pyr15TM at pH 6.1 and the 2′,4′-BNA^{NC}-modified TFOs at pH 6.8 with similar stoichiometry

will provide reasonable promotion mechanism of the triplex formation by the 2′,4′-BNA^{NC} modification of TFO, as discussed in the following.

Although the K_a and ΔG for Pyr15TM at pH 6.1 and those for the 2′,4′-BNA^{NC}-modified TFOs at pH 6.8 were quite similar (Table 4), the constituents of ΔG, that is, ΔH and ΔS, were obviously different. The magnitudes of the negative ΔH and ΔS for the 2′,4′-BNA^{NC}-modified TFOs at pH 6.8 were smaller than those observed for Pyr15TM at pH 6.1 (Table 4). The observed negative ΔH upon the triplex formation reflects major contributions from the hydrogen bonding and the base stacking involved in the triplex formation, the protonation of the cytosine bases upon the hydrogen bonding, and the accompanying deprotonation of the cacodylate buffer releasing the protons to bind with the cytosine bases[33-35]. The immobilization of electrostricted water molecules around polar atoms upon the triplex formation is also considered to be the major sources of the observed negative ΔH upon the triplex formation[33-35]. Because the degree of the protonation may be similar between the 2′,4′-BNA^{NC}-modified TFOs at pH 6.8 and Pyr15TM at pH 6.1 due to the similar stoichiometry discussed above and the protons to bind with the cytosine bases are released from the same cacodylate buffer in both cases, the ΔH derived from the protonation of the cytosine bases and the accompanying deprotonation of the cacodylate buffer should be similar between the two cases. Also, the CD spectra showed that the higher-order structure of the triplexes with each of the 2′,4′-BNA^{NC}-modified TFOs was quite similar to that with the corresponding unmodified TFO (Figure 3), suggesting no significant change in the hydrogen bonding and/or the base stacking of the triplex by the 2′,4′-BNA^{NC}-modification. Thus, the difference in ΔH between the 2′,4′-BNA^{NC}-modified TFOs at pH 6.8 and Pyr15TM at pH 6.1 (Table 4) should mainly result from the contribution that the 2′,4′-BNA^{NC}-modification may change the degree of the immobilization of water molecules around the polar atoms of the triplex. The polar nitrogen atom in the aminomethylene chain to bridge 2′-O and 4′-C of the sugar moiety may possibly achieve such change. On the other hand, the observed ΔS upon the triplex formation is mainly contributed by the two factors, a negative conformational entropy change due to the conformational restraint of TFO involved in the triplex formation, and a positive dehydration entropy change from the release of structured water molecules surrounding the TFO and the target duplex upon the triplex formation[33-35]. Therefore, one of the reason for the smaller magnitudes of the negative ΔS for the 2′,4′-BNA^{NC}-modified TFOs at pH 6.8 in comparison with that for Pyr15TM at pH 6.1 (Table 4) may be based on the negative conformational entropy change. The 2′,4′-BNA^{NC}-modified TFO in the free state may be more rigid than the corresponding unmodified TFO, because the 2′-O and 4′-C positions of the sugar moiety of the 2′,4′-BNA^{NC} are bridged with the aminomethylene chain. The increased rigidity in the free state may cause the smaller loss of the conformational entropy upon the triplex formation with the 2′,4′-BNA^{NC}-modified TFO. Another reason for the smaller magnitudes of the negative ΔS for the 2′,4′-BNA^{NC}-modified TFOs at pH 6.8 relative to that for Pyr15TM at pH 6.1 (Table 4) may be derived from the positive dehydration entropy change. The nitrogen atom in the aminomethylene chain may result in the increased degree of hydration of the 2′,4′-BNA^{NC}-modified TFO in the free state. The increased degree of hydration in the free state may cause the larger gain of the dehydration entropy upon the triplex formation with the 2′,4′-BNA^{NC}-modified TFO. We

conclude that the smaller loss of the conformational entropy due to the increased rigidity in the free state and the larger gain of the dehydration entropy due to the increased degree of hydration in the free state may result in the smaller magnitudes of the negative ΔS for the 2′,4′-BNA^{NC}-modified TFOs at pH 6.8, which provides a favorable component to the ΔG and leads to the increase in the K_a of the triplex formation at neutral pH.

The increase in the K_a by the 2′,4′-BNA^{NC} modification was similar in magnitude among the four modified TFOs (Figure 4 and Tables 4 and 5), indicating that the number and position of the 2′,4′-BNA^{NC} modification did not significantly affect the magnitude of the increase in the K_a at neutral pH. The increased rigidity and the increased degree of hydration themselves of the 2′,4′-BNA^{NC}-modified TFO may be more important to achieve the increase in the K_a at neutral pH than the variation of the number and position of the 2′,4′-BNA^{NC} modification. Thus, other modification strategies to gain the increased rigidity of TFO and the increased degree of hydration of TFO may be also useful to increase the K_a at neutral pH.

Kinetic data have demonstrated that the 2′,4′-BNA^{NC} modification of TFO considerably decreased the k_{dissoc} of the pyrimidine motif triplex formation at neutral pH (Table 5). The decrease in the k_{dissoc} is a plausible kinetic reason to explain the remarkable gain in the K_a at neutral pH by the 2′,4′-BNA^{NC} modification (Figure 4 and Tables 4 and 5). Both our group[35] and others[36] have previously proposed a model that triplexes form along nucleation-elongation processes: in a nucleation step only a few base contacts of the Hoogsteen hydrogen bonds may be formed between TFO and the target duplex, and this may be followed by an elongation step in which Hoogsteen base pairings progress to complete triplex formation. Both groups[35,36] have also suggested that the observed K_a, which is the ratio of k_{assoc} to k_{dissoc}, may mostly reflect a rapid equilibrium of the nucleation step, which is probably the rate-limiting process of the triplex formation. In this sense, the 2′,4′-BNA^{NC} modification is considered to slow the collapse of the nucleation intermediate using the increased rigidity and the increased degree of hydration of 2′,4′-BNA^{NC}-modified TFO to increase the K_a of the pyrimidine motif triplex formation.

The nuclease resistance of the 2′,4′-BNA^{NC}-modified TFO in human serum was significantly higher than that of the unmodified TFO (Figures 7 and 8). The 2′,4′-BNA^{NC} modification increased the nuclease resistance of TFOs in human serum. Previously, the nuclease resistance of the phosphorothioate backbone, in which a nonbridging oxygen of a phosphodiester group was replaced by a sulfur atom, was known to be significantly higher than that of the unmodified backbone[37,38]. However, the K_a of the triplex formation with the phosphorothioate modified TFO was significantly smaller than that with the unmodified TFO[39,40]. Thus, the phosphorothioate modification increased the nuclease resistance of TFO, but it decreased the triplex forming ability. On the other hand, as discussed above, the 2′,4′-BNA^{NC} modification of TFO increased the triplex forming ability at neutral pH (Figure 4 and Tables 4 and 5). Therefore, the 2′,4′- BNA^{NC} modification enhanced both the nuclease resistance of TFO and the triplex forming ability at neutral pH. We conclude that due to these excellent properties the 2′,4′-BNA^{NC} modification may be more favorable than the phosphorothioate modification upon the application of TFO to the various triplex formation-based strategies *in vivo*.

The 2′,4′-BNA^{NC}-modified antisense oligonucleotides showed the excellent antisense effect to reduce the expression level of PCSK9 mRNA (Figure 9). As discussed above, the 2′,4′-BNA^{NC}-modified oligonucleotides exhibited significantly higher binding affinity with complementary ssRNA than unmodified oligonucleotides (Table 1). Also, the 2′,4′-BNA^{NC} modification significantly increased the nuclease resistance of oligonucleotides in human serum (Figures 7 and 8). The significantly higher binding affinity with complementary ssRNA and the significantly higher nuclease resistance of oligonucleotides in human serum may achieve the excellent antisense effect of the 2′,4′-BNA^{NC}-modified antisense oligonucleotides. We conclude that the 2′,4′-BNA^{NC}-modified antisense oligonucleotides may be useful to reduce the expression level of the target mRNA.

12. Conclusion

The present study has clearly indicated that the 2′,4′-BNA^{NC} modification increased the thermal stability of the duplex with complementary ssRNA and ssDNA at neutral pH. It has also clearly demonstrated that the 2′,4′-BNA^{NC} modification of TFO increased not only the thermal stability of the pyrimidine motif triplex but also the K_a of the pyrimidine motif triplex formation at neutral pH by more than 10-fold, which mainly resulted from the considerable decrease in the k_{dissoc}. It has also revealed that the 2′,4′-BNA^{NC} modification of TFO significantly increased the nuclease resistance of TFO in human serum. Our results certainly support the idea that the 2′,4′-BNA^{NC}-modified oligonucleotides may have a potential to be applied to the various duplex and triplex formation-based strategies *in vivo*, such as regulation of gene expression by antisense and antigene technology, mapping of genomic DNA, and gene-targeted mutagenesis. In fact, the 2′,4′-BNA^{NC}-modified antisense oligonucleotides showed the excellent antisense effect to reduce the expression level of the target mRNA. In addition, the present study has revealed that the increased rigidity and the increased degree of hydration of the 2′,4′-BNA^{NC}-modified TFO in the free state may enable the significant increase in the K_a for the pyrimidine motif triplex formation at neutral pH. We conclude that the design of oligonucleotides to bridge different positions of sugar moiety with polar atom-containing alkyl chain for the increased rigidity and the increased degree of hydration is certainly a promising strategy for the promotion of the duplex and triplex formation under physiological condition, and may eventually lead to progress in various duplex and triplex formation-based strategies *in vivo*.

Author details

Hidetaka Torigoe*
Department of Applied Chemistry, Faculty of Science, Tokyo University of Science, Shinjuku-ku, Tokyo, Japan

Takeshi Imanishi
Graduate School of Pharmaceutical Sciences, Osaka University, Suita, Osaka, Japan
BNA Inc., Ibaraki, Osaka, Japan

* Corresponding Author

Acknowledgement

We thank Dr. S. M. Abdur Rahman, Dr. Kiyomi Sasaki, Ms. Hiroko Takuma, Ms. Sayori Seki, and Mr. Haruhisa Yoshikawa for their technical assistance. We acknowledge Prof. Satoshi Obika and Prof. Kazuyuki Miyashita for their useful discussions. The present work was supported in part by Grant-in-Aid for Scientific Research on Innovative Areas (22113519), Grant-in-Aid for Exploratory Research (20655038), Grant-in-Aid for Scientific Research (B) (21350094) and Grant-in-Aid for JSPS Fellows (22-10383) from the Ministry of Education, Science, Sports, and Culture of Japan. This work was also supported partly by the Program for Promotion of Fundamental Studies in Health Sciences of the National Institute of Biomedical Innovation (NIBIO), the Program for Precursory Research for Embryonic Science and Technology (PRESTO), and the Creation and Support Program for Start-ups from the Universities of the Japan Science and Technology Agency (JST)

13. References

[1] Kole R, Krainer AR,Altman S (2012) Rna Therapeutics: Beyond Rna Interference and Antisense Oligonucleotides. Nat Rev Drug Discov. 11: 125-140.

[2] Watts JK,Corey DR (2012) Silencing Disease Genes in the Laboratory and the Clinic. J Pathol. 226: 365-379.

[3] Duca M, Vekhoff P, Oussedik K, Halby L,Arimondo PB (2008) The Triple Helix: 50 Years Later, the Outcome. Nucleic Acids Res. 36: 5123-5138.

[4] Jain A, Wang G,Vasquez KM (2008) DNA Triple Helices: Biological Consequences and Therapeutic Potential. Biochimie. 90: 1117-1130.

[5] Frank-Kamenetskii MD (1992) Protonated DNA Structures. Methods Enzymol. 211: 180-191.

[6] Singleton SF,Dervan PB (1992) Influence of Ph on the Equilibrium Association Constants for Oligodeoxyribonucleotide-Directed Triple Helix Formation at Single DNA Sites. Biochemistry. 31: 10995-11003.

[7] Shindo H, Torigoe H,Sarai A (1993) Thermodynamic and Kinetic Studies of DNA Triplex Formation of an Oligohomopyrimidine and a Matched Duplex by Filter Binding Assay. Biochemistry. 32: 8963-8969.

[8] Wickstrom E (1986) Oligodeoxynucleotide Stability in Subcellular Extracts and Culture Media. J Biochem Biophys Methods. 13: 97-102.

[9] Prakash TP (2011) An Overview of Sugar-Modified Oligonucleotides for Antisense Therapeutics. Chem Biodivers. 8: 1616-1641.

[10] Rahman SM, Seki S, Obika S, Haitani S, Miyashita K,Imanishi T (2007) Highly Stable Pyrimidine-Motif Triplex Formation at Physiological Ph Values by a Bridged Nucleic Acid Analogue. Angew Chem Int Ed Engl. 46: 4306-4309.

[11] Rahman SM, Seki S, Obika S, Yoshikawa H, Miyashita K,Imanishi T (2008) Design, Synthesis, and Properties of 2',4'-Bna(Nc): A Bridged Nucleic Acid Analogue. J Am Chem Soc. 130: 4886-4896.

[12] Torigoe H, Rahman SM, Takuma H, Sato N, Imanishi T, Obika S,Sasaki K (2011) 2'-O,4'-C-Aminomethylene-Bridged Nucleic Acid Modification with Enhancement of Nuclease Resistance Promotes Pyrimidine Motif Triplex Nucleic Acid Formation at Physiological Ph. Chemistry. 17: 2742-2751.

[13] Torigoe H, Rahman SM, Takuma H, Sato N, Imanishi T, Obika S,Sasaki K (2011) Interrupted 2'-O,4'-C-Aminomethylene Bridged Nucleic Acid Modification Enhances Pyrimidine Motif Triplex-Forming Ability and Nuclease Resistance under Physiological Condition. Nucleosides Nucleotides Nucleic Acids. 30: 63-81.

[14] Yamamoto T, Harada-Shiba M, Nakatani M, Wada S, Yasuhara H, Narukawa K, Sasaki K, Shibata M, Torigoe H, Yamaoka T, Imanishi T,Obika S (2012) Cholesterol-Lowering Action of Bna-Based Antisense Oligonucleotides Targeting Pcsk9 in Atherogenic Diet-Induced Hypercholesterolemic Mice. Molecular Therapy-Nucleic Acids. 1: e22.

[15] Mousavi SA, Berge KE,Leren TP (2009) The Unique Role of Proprotein Convertase Subtilisin/Kexin 9 in Cholesterol Homeostasis. J Intern Med. 266: 507-519.

[16] Abifadel M, Rabes JP, Devillers M, Munnich A, Erlich D, Junien C, Varret M,Boileau C (2009) Mutations and Polymorphisms in the Proprotein Convertase Subtilisin Kexin 9 (Pcsk9) Gene in Cholesterol Metabolism and Disease. Hum Mutat. 30: 520-529.

[17] Soutar AK (2010) Rare Genetic Causes of Autosomal Dominant or Recessive Hypercholesterolaemia. IUBMB Life. 62: 125-131.

[18] Riley M,Maling B (1966) Physical and Chemical Characterization of Two- and Three-Stranded Adenine-Thymine and Adenine-Uracil Homopolymer Complexes. J Mol Biol. 20: 359-389.

[19] Torigoe H, Ferdous A, Watanabe H, Akaike T,Maruyama A (1999) Poly(L-Lysine)-Graft-Dextran Copolymer Promotes Pyrimidine Motif Triplex DNA Formation at Physiological Ph. Thermodynamic and Kinetic Studies. J Biol Chem. 274: 6161-6167.

[20] Torigoe H, Hari Y, Sekiguchi M, Obika S,Imanishi T (2001) 2'-O,4'-C-Methylene Bridged Nucleic Acid Modification Promotes Pyrimidine Motif Triplex DNA Formation at Physiological Ph: Thermodynamic and Kinetic Studies. J Biol Chem. 276: 2354-2360.

[21] Torigoe H (2001) Thermodynamic and Kinetic Effects of N3'-->P5' Phosphoramidate Modification on Pyrimidine Motif Triplex DNA Formation. Biochemistry. 40: 1063-1069.

[22] Torigoe H,Maruyama A (2001) Promotion of Duplex and Triplex DNA Formation by Polycation Comb-Type Copolymers. Methods Mol Med. 65: 209-224.

[23] Torigoe H,Maruyama A (2005) Synergistic Stabilization of Nucleic Acid Assembly by Oligo-N3'-->P5' Phosphoramidate Modification and Additions of Comb-Type Cationic Copolymers. J Am Chem Soc. 127: 1705-1710.

[24] Torigoe H, Maruyama A, Obika S, Imanishi T,Katayama T (2009) Synergistic Stabilization of Nucleic Acid Assembly by 2'-O,4'-C-Methylene-Bridged Nucleic Acid Modification and Additions of Comb-Type Cationic Copolymers. Biochemistry. 48: 3545-3553.

[25] Torigoe H, Sasaki K,Katayama T (2009) Thermodynamic and Kinetic Effects of Morpholino Modification on Pyrimidine Motif Triplex Nucleic Acid Formation under Physiological Condition. J Biochem. 146: 173-183.

[26] Torigoe H, Nakagawa O, Imanishi T, Obika S,Sasaki K (2012) Chemical Modification of Triplex-Forming Oligonucleotide to Promote Pyrimidine Motif Triplex Formation at Physiological Ph. Biochimie. 94: 1032-1040.
[27] Torigoe H, Sato N,Nagasawa N (2012) 2′-O,4′-C-Ethylene Bridged Nucleic Acid Modification Enhances Pyrimidine Motif Triplex Forming Ability under Physiological Condition. J Biochem. in press.
[28] Wiseman T, Williston S, Brandts JF,Lin LN (1989) Rapid Measurement of Binding Constants and Heats of Binding Using a New Titration Calorimeter. Anal Biochem. 179: 131-137.
[29] Bates PJ, Dosanjh HS, Kumar S, Jenkins TC, Laughton CA,Neidle S (1995) Detection and Kinetic Studies of Triplex Formation by Oligodeoxynucleotides Using Real-Time Biomolecular Interaction Analysis (Bia). Nucleic Acids Res. 23: 3627-3632.
[30] Edwards PR, Gill A, Pollard-Knight DV, Hoare M, Buckle PE, Lowe PA,Leatherbarrow RJ (1995) Kinetics of Protein-Protein Interactions at the Surface of an Optical Biosensor. Anal Biochem. 231: 210-217.
[31] Manzini G, Xodo LE, Gasparotto D, Quadrifoglio F, van der Marel GA,van Boom JH (1990) Triple Helix Formation by Oligopurine-Oligopyrimidine DNA Fragments. Electrophoretic and Thermodynamic Behavior. J Mol Biol. 213: 833-843.
[32] Lyamichev VI, Mirkin SM, Frank-Kamenetskii MD,Cantor CR (1988) A Stable Complex between Homopyrimidine Oligomers and the Homologous Regions of Duplex Dnas. Nucleic Acids Res. 16: 2165-2178.
[33] Edelhoch H,Osborne JC, Jr. (1976) The Thermodynamic Basis of the Stability of Proteins, Nucleic Acids, and Membranes. Adv Protein Chem. 30: 183-250.
[34] Cheng YK,Pettitt BM (1992) Stabilities of Double- and Triple-Strand Helical Nucleic Acids. Prog Biophys Mol Biol. 58: 225-257.
[35] Kamiya M, Torigoe H, Shindo H,Sarai A (1996) Temperature Dependence and Sequence Specificity of DNA Triplex Formation: An Analysis Using Isothermal Titration Calorimetry. J Am Chem Soc. 118: 4532-4538.
[36] Rougee M, Faucon B, Mergny JL, Barcelo F, Giovannangeli C, Garestier T,Helene C (1992) Kinetics and Thermodynamics of Triple-Helix Formation: Effects of Ionic Strength and Mismatches. Biochemistry. 31: 9269-9278.
[37] Zon G,Geiser TG (1991) Phosphorothioate Oligonucleotides: Chemistry, Purification, Analysis, Scale-up and Future Directions. Anticancer Drug Des. 6: 539-568.
[38] Stein CA, Tonkinson JL,Yakubov L (1991) Phosphorothioate Oligodeoxynucleotides--Anti-Sense Inhibitors of Gene Expression? Pharmacol Ther. 52: 365-384.
[39] Xodo L, Alunni-Fabbroni M, Manzini G,Quadrifoglio F (1994) Pyrimidine Phosphorothioate Oligonucleotides Form Triple-Stranded Helices and Promote Transcription Inhibition. Nucleic Acids Res. 22: 3322-3330.
[40] Torigoe H, Shimizume R, Sarai A,Shindo H (1999) Triplex Formation of Chemically Modified Homopyrimidine Oligonucleotides: Thermodynamic and Kinetic Studies. Biochemistry. 38: 14653-14659.